Three-dimensional synchrotron x-ray particle image velocimetry

A. Fouras[a)]
Division of Biological Engineering, Monash University, P.O. Box 31, Melbourne 3800, Australia

J. Dusting
Department of Mechanical Engineering, Monash University, P.O. Box 31, Melbourne 3800, Australia

R. Lewis
Monash University Center for Synchrotron Science, Monash University, P.O. Box 27, Melbourne 3800, Australia

K. Hourigan
Division of Biological Engineering, Monash University, P.O. Box 31, Melbourne 3800, Australia

(Received 19 September 2006; accepted 3 August 2007; published online 28 September 2007)

There is great potential to vastly improve biological flow measurement by using a combination of synchrotron imaging and the latest experimental flow measurement techniques. In the current paper, the three-dimensional velocity field within a cylindrical tube is measured using a combination of phase-contrast x-ray imaging and particle image velocimetry (PIV). We greatly refine the techniques previously used to undertake velocity measurements with a synchrotron light source, substantially enhancing accuracy. Furthermore a PIV correlation peak analysis is developed to allow three-dimensional measurement of the velocity field. © *2007 American Institute of Physics*.
[DOI: 10.1063/1.2783978]

I. INTRODUCTION

The potential applications for three-dimensional flow resolution inside closed, opaque vessels are numerous and significant. For instance, the detailed measurement of flow fields within blood vessels would facilitate more advanced research into the role of hemodynamics in the development and potential treatment of cardiovascular disease. Diseased conditions of the vasculature such as stenosis and aneurysm are the continued focus of much research.[1,2] Techniques to measure the fluid dynamics properties of the blood flow through the effected vascalature with increased resolution and accuracy are key to developing treatments and understanding of these diseases.[3–6] Many current blood flow measurement techniques can only quantify peak systolic velocity, a single indicator of the average flow field. Fully three-dimensional (3D) velocity measurements would also yield a number of more useful flow parameters such as flow rate, wall shear, and turbulence levels. Other possible biomedical applications include the study of flow through optically opaque heart valves and artificial hearts, both of which are challenging flow geometries to evaluate.

The ability to resolve the instantaneous velocity field across a 3D volume is a highly desirable technology that has alluded fluid mechanics experimentalists. Three-dimensional holographic particle image velocimetry (PIV) has reportedly been used to measure instantaneous turbulent flow fields in three dimensions,[7] but this technique has several shortcomings. These include an immensely complex optical setup for data acquisition and reconstruction,[8] a very poor signal to noise ratio, and the inability to record a time sequence of velocity fields. Scanned, multiplane PIV (Ref. 9) or stereoscopic particle image velocimetry[10] (SPIV) can be used to compile 3D flow fields; however, scanning techniques require the data within each plane to be captured at different points in time and therefore necessitate the interrogated flow to be stationary in time.

It is problematic to measure flows within opaque vessels, such as blood vessels, using current technologies. Most common spatially resolved flow measurement techniques, such as PIV or SPIV, require clear optical access to the region of interest. Medical imaging techniques that have previously been used to measure flows *in vivo*, such as ultrasonography and magnetic resonance imaging (MRI), are generally restricted to velocity field measurements with spatial resolutions of millimeter precision.

X-ray imaging has also rarely been applied to flow measurement. Seeger *et al.*[11] tracked individual particles in a bubble column in 3D space using dual x-ray detector systems. In general, though, particle tracking velocimetry (PTV) leads to low levels of information being recorded as it relies on identification of individual tracers that must be present in low numbers, especially when used with volume illumination. Lee and Kim subsequently used PIV rather than PTV and achieved far more measurements.[12] PIV is a newer flow measurement technique than PTV, however, it is well established within the field of fluid mechanics. Importantly it has been shown to be capable of accurately measuring instantaneous velocity fields that have a high dynamic range. In PIV, regions of fluid containing multiple tracer particles are imaged at two points in time separated by a known time interval and processed using correlation software. This process produces correlation "peaks" at separate sampling window locations across the interrogation region, which are then converted into velocity vectors by assuming that the mode value

[a)]Electronic mail: fouras@eng.monash.edu

represents the average velocity within the window. As it is statistically based, PIV can work with poorer signal to noise ratios and higher particle numbers than PTV.

Using an x-ray light source to conduct PIV poses its own significant problems, especially due to the fact that the fluid region is volume illuminated. In PIV, the light source is ideally narrowed to a flat plane, meaning that only a single cross section of the flow is interrogated and any velocity variations in the out-of-plane (or z) direction are not recorded. As the light sheet is thickened, the velocity variation in z is included within the imaged region and contaminates the PIV signal. This is particularly serious for flows that are significantly variable in the out-of-plane direction, such as a pipe flow viewed from the side. As Lee and Kim[13] used a flow with a Poiseuille velocity profile, they were only capable of measuring pipe flow in a z-averaged sense. The problem of volume illumination is also currently endemic to micro-PIV.[14,15] The amount of information contaminating the flow from outside the desired imaging plane is a function of the depth of focus and is therefore mostly controlled by the numerical aperture of the microscope lens. This makes resolution of velocity data in the z direction from a volume-averaged cross-correlated particle field even more advantageous.

Synchrotron phase-contrast x-ray imaging is a powerful tool for anatomical measurement and offers much improved contrast over conventional imaging for biological tissues.[16,17]

In the current paper we develop a PIV correlation peak analysis combined with phase-contrast x-ray imaging to measure 3D velocity fields. Research in developing the technique exposes flaws in the way previous volume-averaged x-ray PIV has been undertaken.

II. 2D X-RAY PIV

PIV is a well established tool for measuring the displacement of tracer particles within a measurement plane.[18] The two-dimensional (2D) region imaged by a camera is typically illuminated over a limited depth by the use of a thin laser sheet, allowing the statistical (2D) measurement to be applicable to any region of flow that is approximately 2D. This process works by discretizing the 2D image into sampling windows and performing a cross-correlation analysis between the sampling windows of frames taken a short time interval (Δt) apart. The peak in the cross correlation typically represents the modal displacement inside the measurement volume over the time between exposures. The representative velocity inside that sampling window at that time is then simply the ratio of the displacement and the time separation.

Local variation in the peak is mainly due to the statistical certainty of noninteger displacements; interrogation of the local variation of the peak yields an estimate of subpixel component of the displacement.[19] The width of the signal peak is typically twice the length of the particle diameter. In the unusual case where there are large displacement gradients inside the imaging plane, the peak is smeared by these gradients. The common solution to this is to estimate the gradients and distort the image to deconvolve, or "unsmear," the peak against these distortions[20] improving the signal to noise ratio.

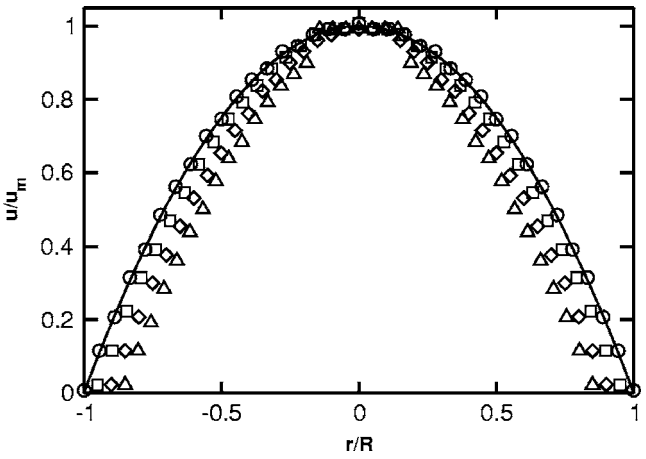

FIG. 1. Profiles calculated by taking the modal velocity inside discrete windows of a simulated 3D pipe flow data field. The different symbols represent different sampling window sizes. ○ symbols represent $S/R=10^{-3}$; □ symbols represent $S/R=0.05$; ◇ symbols represent $S/R=0.10$; and △ symbols represent $S/R=0.15$. For comparison, the exact maximum u profile is plotted as a solid line.

Lee and Kim,[13] have reported the 2D measurement of a duct flow using x-ray PIV. While the flow in the axial (x) and vertical (y) axes was presented, the flow in the out-of-plane direction (z) was not shown. However, any gradients in the z direction will certainly contribute to variation of the correlation peaks from which the 2D measurement was derived. Lee and Kim understood this and explained their substantial underestimation of the velocity field as being caused by the PIV measurement representing the mean velocity. However, PIV measures the modal, rather than the mean, velocity at each window location.

Figure 1 shows computer modeling of the modal velocity at spanwise locations across a cylindrical tube at low Reynolds numbers (Re). The Reynolds number represents the ratio of momentum and viscous fluid forces and is calculated as $\mathrm{Re}=uD/v$ where u is the velocity, D is the pipe diameter, and v is the kinematic viscocity of the fluid. The velocity in the radial and azimuthal directions is assumed to be 0, while the axial flow, given by velocity u, is assumed to be parabolic in nature. That is,

$$u/u_m = 1 - r^2/R^2, \tag{1}$$

where u_m is the maximum axial velocity, r is the radial position from the tube axis of symmetry, and R is the total radius of the tube. For the simulation, a representative circular cross section of the pipe flow was discretized into 5000 $\times$ 5000 points, which were then used to develop histograms. The modal values within discrete windows of varying size S are plotted in Fig. 1 as a function of the window midpoint location in the r direction. For this flow configuration, the modal velocity is very nearly equal to the maximum velocity, with any difference caused by the finite histogram bin size. The underestimation visible at the edges of the figure is a function of the finite size of the window. This effect increases as the relative window size increases. Lee and Kim were subject to a similar underestimation phenomenon in their data, but attributed it to the sinking of tracer particles near the wall. However, the terminal velocity of relatively

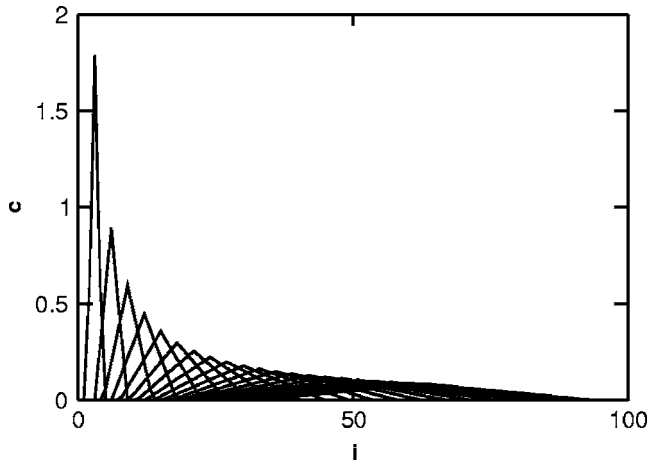

FIG. 2. Sequence of functions (c) depicting convolution matrix C as a function of displacement component i. Note that the area under each triangle is constant. The experiments conducted as part of this study have $\epsilon_\tau = 0.495$.

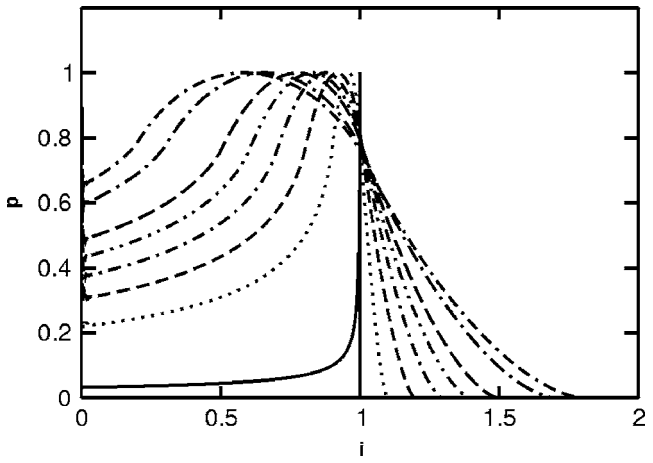

FIG. 3. Theoretical peak constructed from the PDF of center line Poiseuille circular pipe flow, with peaks convolved by convolution functions constructed with ϵ_τ varying from 0.1 to 0.7. In each case the peak magnitude p is plotted as a function of displacement component i. The solid line represents the theoretical peak, ··· represents $\epsilon_\tau=0.1$, --- represents $\epsilon_\tau=0.2$, -·-· represents $\epsilon_\tau=0.3$, -···- represents $\epsilon_\tau=0.4$, — — represents $\epsilon_\tau=0.5$, —·— represents $\epsilon_\tau=0.6$, and ·– –· represents $\epsilon_\tau=0.7$.

heavy particles would not be more significant near the wall than at the center, and the underestimation in their data is more likely due to the finite window size effect.

The underestimation of peak velocity for finite window sizes is, in fact, related to a completely different phenomenon than sinking tracer particles. Typically PIV is performed using pulsed lasers. These lasers deliver a moderate amount of light energy in an extremely short period of time, characteristically a few nanoseconds. This means that the exposure time (effectively the pulse duration for a pulsed light source) is very short compared to the time between exposures. However, when performing x-ray PIV with a synchrotron light source, particle images will be smeared by the motion captured by the psuedocontinuous illumination. This smears the correlation peaks in a manner proportional to the particle velocity. As there are multiple velocities present within each window, the smearing of the correlation peaks becomes complex.

In the technique developed here, each velocity component is considered separately and convolved by a function that is itself a function of the velocity. These functions are easily derived with an analytical consideration of the cross correlation of top-hat functions. The length of the top-hat function is given by the product of the velocity (u) and exposure time, and the displacement is given by the product of u and Δt. These equations can be conveniently nondimensionalized by the use of the term ϵ_τ, the ratio of the exposure time to Δt.

Each smeared particle image can be approximated by a top-hat function. The cross-correlation peak of two top-hat functions is triangular, and since each volumetric region contributes equally to the peak, the area under each triangle is fixed. The higher the velocity, the longer the top hat, and the longer and therefore lower the triangle. As an illustration of this concept, Fig. 2 shows a number of the functions $c(i,j)$ that make up the convolution matrix C. As the displacement increases, the response becomes broader, with a lower maximum value. When a range of displacement components is present, this results in a bias toward the lower displacement components, and hence a potential underestimation of velocity.

Figure 3 shows how a theoretical peak, which also represents a probability density function of displacement, is smeared by the convolution functions with varying ϵ_τ. A shift of the peak toward zero caused by the convolution process is clearly visible. This shift is approximately proportional to ϵ_τ, the ratio of exposure time t_e, and time between exposures Δt. Figure 4 demonstrates the extent to which the peak value moves as a function of ϵ_τ. It is evident that the process is nearly linear.

Since we know that the peak shifting effect is approximately linear with ϵ_τ, we can establish a new technique for its removal. This involves solving for the velocity field twice and then using a technique similar to Richardson's extrapolation to solve for the correct velocity. The two estimates for the velocity are obtained by using two distinct time intervals

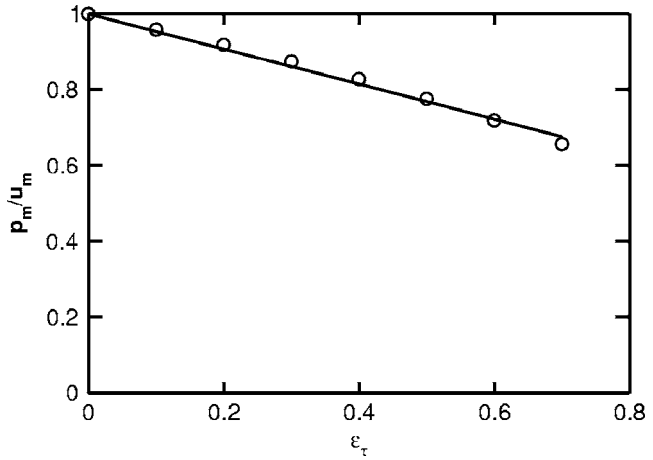

FIG. 4. Relative i position maximum value of peak as a function of ϵ_τ, for Poiseuille circular pipe flow. A regression line is also included to demonstrate the extent to which the phenomenon is linear.

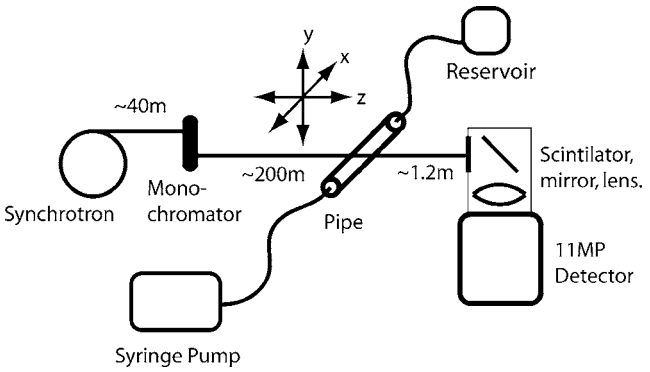

FIG. 5. Schematic of the synchrotron x-ray PIV and pipe flow system, as well as the coordinate system.

over which to perform the PIV process. For the current study we used frame intervals of 1 and 2 frames. This means that the PIV process was integrated between frames 1 and 2, 2 and 3, and so on for an interval of 1, and between 1 and 3 and 2 and 4, and so on for a frame interval of 2.

Mathematically, the solution to the problem can be expressed as in Eq. (2), where k is a constant specific to the velocity profile. This equation shows that by extrapolating between the two estimates of displacement, Δx_1 and Δx_2, a velocity estimate (Δx) without an ϵ_τ error term can be evaluated.

$$\Delta x_1 = u\Delta t + kt_e/\Delta t,$$

$$\Delta x_2 = 2[u\Delta t + kt_e/(2\Delta t)],$$

$$\Delta x = u\Delta t = \Delta x_2 - \Delta x_1. \tag{2}$$

This technique is simple to implement and means that in future x-ray PIV practitioners will be able to achieve simple two-dimensional measurements with a synchrotron light source. The authors have completed this analysis for the flow in a round pipe at $\mathrm{Re} \approx 10^{-4}$. This flow was achieved in a 15 mm diameter pipe filled with glycerin containing silver coated hollow glass microspheres (Potters Industries). The glycerin was pumped through the pipe using a syringe pump.

The experiments were conducted at the Spring8 synchrotron with the approval of the Japan Synchrotron Radiation Research Institute (JASRI). The experiments were conducted on the biomedical beam-line(20B2) with a 25 keV x-ray beam that was approximately 25 mm in height and 40 mm in width. The images were acquired with a Hamamatsu beam monitor (BM4) with 4000×2642 pixels and a pixel size of 5.87 μm. The exposures used were 2940 ms and the exposure delay was 5940 ms (ϵ_τ=0.495). Figure 5 shows the basic layout of the experiment and coordinate system.

Figure 6 shows a portion of the measured 2D velocity field presented for clarity at reduced resolution. Those familiar with PIV will recognize the spatial resolution of the flow displayed in a 2D sense. Since the beam is parallel and the flow is steady, we expect to see no variation of the flow in the x (streamwise) direction. The flow qualitatively agrees with the theoretical flow of Eq. (1). As expected, little or no variation in x is visible and a variation from very low flow at the wall to peak flow at the center line can be seen.

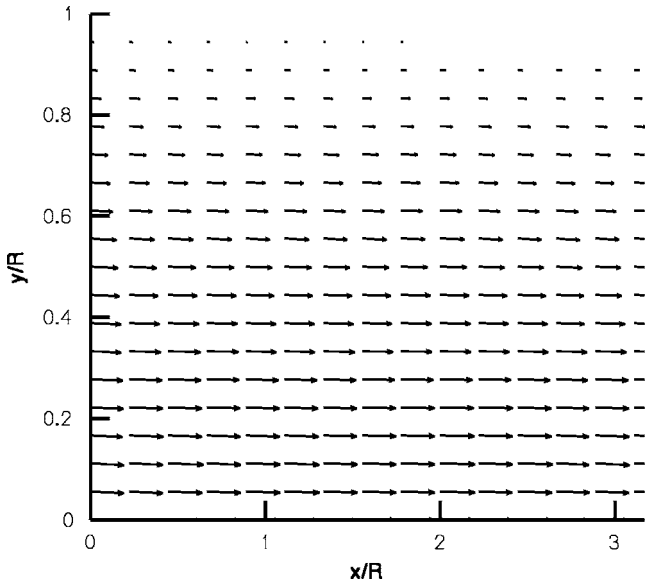

FIG. 6. Measured two-dimensional velocity vector field prior to peak analysis. For clarity, only the upper half of the vessel and every fourth vector are shown. The actual resolution is 59×37 vectors.

For a more quantitative evaluation of the technique, the calculated maximum flow profile is compared to the measured profile in Fig. 7. For completeness, measured profiles from the two estimates used to calculate the actual velocity are also shown. The excellent agreement between the measured maximum velocity and the theoretical value is clear. As described above, the slight underestimation near the walls is to be expected.

III. DECONVOLUTION OF PEAK SMEARING

By interrogating the correlation peak, further information can be extracted relating to the velocity gradients in the measurement volume of each window. As mentioned above, the relatively long exposure times required for synchrotron imaging smear the correlation peak, causing distortion of ve-

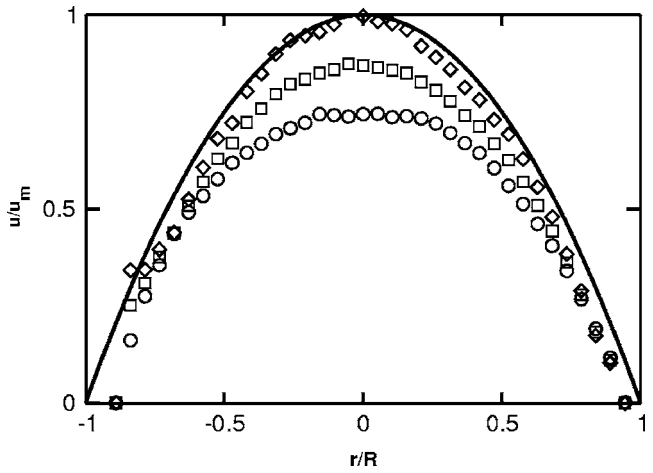

FIG. 7. Measured average velocity profile based on different cross-correlation peaks: ○ symbols represent velocities achieved using Δx_1; □ symbols represent velocities achieved using $\Delta x_2/2$; and ◇ symbols represent velocities achieved using Δx. For comparison, the theoretical u profile is plotted as a solid line.

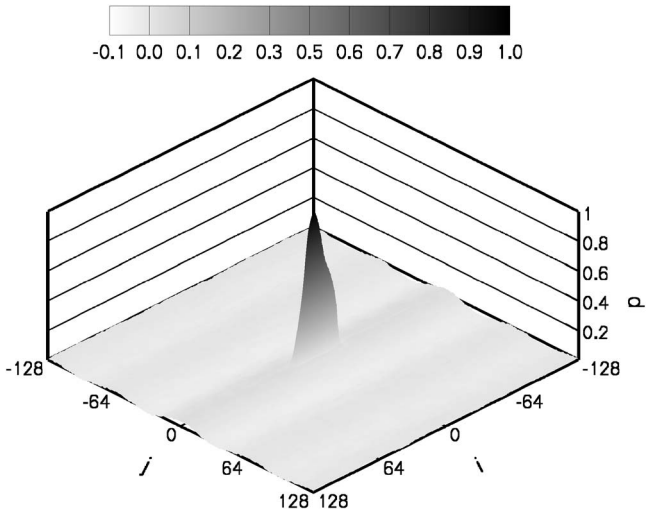

FIG. 8. Average measured two-dimensional cross-correlation peak p_1 corresponding to $y/R=0$, plotted as a function of displacement components i and j. Both the vertical axis and the shading represent the local p magnitude.

locity information and underestimation of peak velocity. Before we can further interrogate the correlation peak, we must first deconvolve the smearing effects to discover the equivalent peak that would result from an instantaneous exposure.

Figure 8 shows p_1, the spatial average of the correlation peaks calculated as part of the evaluation of Δx_1, as a function of the discrete displacement components i and j. In this case, i and j are aligned in the x and y directions, respectively. As shown in Fig. 8, the peak is a thin (two particle diameters wide) linear feature since the velocity gradient is one dimensional. To simplify the analysis, the information in this peak is linearized along the i axis and then, once extracted, displayed as a line plot as in Fig. 9.

Once the data contained in the peak can be visualized in a linear fashion, an extrapolation process to derive the correct peak shape can be easily demonstrated. For this process, we use two peaks, p_1 and p_2, where p_1 results from the analysis of consecutive frames (i.e., 1–2, 2–3, 3–4,…,), and p_2 results from the analysis of every second frame (i.e., 1–3, 2–4, 3–5,…). In a similar manner as one could extrapolate

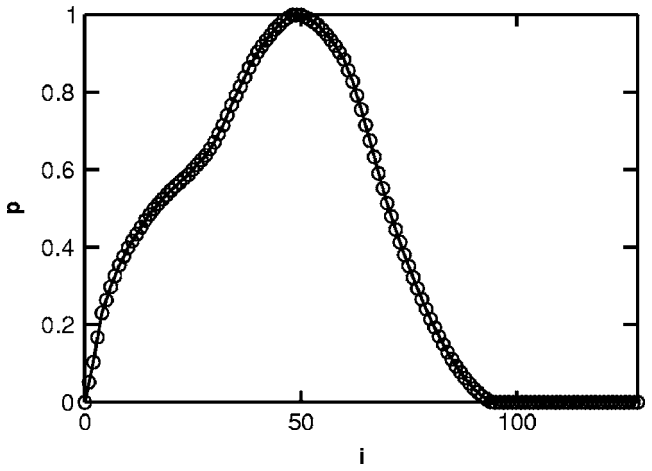

FIG. 9. i cross section of the average measured cross-correlation peak p_1 corresponding to $y/R=0$.

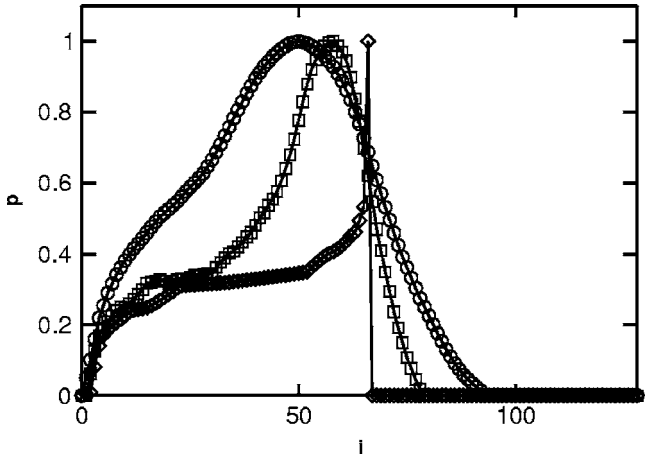

FIG. 10. i cross section of the average measured cross-correlation peaks at $y/R=0$: $2p_1$ (○), p_2 (□), and extrapolated peak $2p_e$ (◇).

from $\Delta x_1, \Delta x_2$ to Δx, we can extrapolate from p_1, p_2 to the extrapolated peak p_e. The linearized plots of $2p_1$, p_2, and $2p_e$ are shown in Fig. 10. The extrapolated peak can be expressed as

$$\delta_e = \delta_2 - \delta_1, \tag{3}$$

where the variable δ represents the i (or displacement coordinate) of a normalized value of the peak. The extrapolated peak shown in Fig. 10 clearly has the same general shape as the theoretical peak shown in Fig. 3.

Now that the correct correlation peak can be reconstructed from Richardson's extrapolation process, it is possible to interrogate the peak to obtain 3D velocity information within the sampling window.

IV. 3D RECONSTRUCTION

As stated previously, each particle contributes to the correlation peak in a position corresponding to its velocity by an amount equal to the intensity of its image. With x-ray imaging there are no depth of focus effects, meaning that every particle contributes equally to the correlation peak. Furthermore, since we can assume in this case that the particle seeding density is equal throughout the volume, we can also assume that the entire flow measurement volume is equally represented in the correlation peak.

We can therefore assert that the correlation peak p_e represents a probability density function (PDF) of the velocity within the measurement volume. This is theoretically as far as the true measurement of the flow can be taken. However, if we can make further assumptions about the flow, then the PDF implies the complete velocity profile. For this particular case, two reasonable assumptions can be made about the flow.

First, we assume that flow near the center line is always greater than flow near the wall. At low and moderate Reynolds numbers, no instability which would violate this assumption will exist. Second, we assume that the flow is symmetric about the plane $z=0$. Given that at each (x,y) location, the same velocity will occur at two z locations, this assumption is necessary unless additional information can be

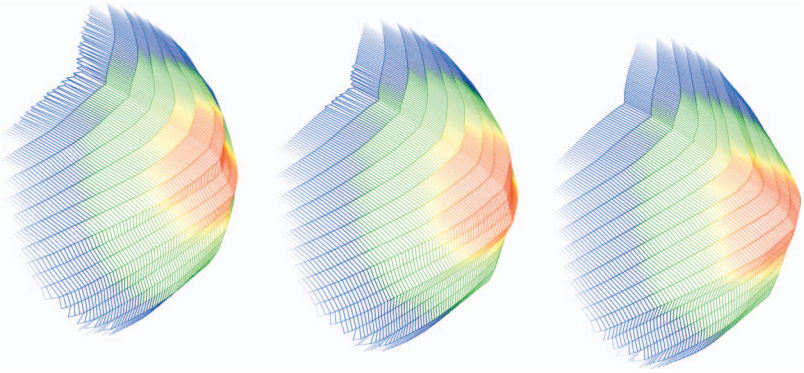

FIG. 11. (Color) Reconstructed three-dimensional velocity field inside a round pipe at a Reynolds number of 10^{-4}. Every node on the mesh corresponds to a different measured value. The colored contours represent the magnitude of u.

provided. The extrema of the z coordinates as a function of x and y are given by $z_m = \pm\sqrt{(R^2 - y^2)}$ as we are using a pipe of fixed radius.

It is now simple to convert the volumetric PDF of the velocity to a velocity profile. We start with the boundary condition corresponding to either the minimum or maximum velocity and integrate along the known displacement values and solve for the z value that matches each displacement. As stated above, in this case we start at $z=0$ for the maximum velocity and at $z=-z_m$ for the minimum velocity,

$$z(u) = z_e \left[1 - \frac{\int_{-\infty}^{u} p(i)di}{\int_{-\infty}^{\infty} p(i)di} \right]. \tag{4}$$

By using the above approach the velocity profile was calculated at each (x,y,z) position inside the pipe over a sequence of 40 frame pairs. These velocities were averaged over time and then plotted as a function of y and z at three different x locations, as shown in Fig. 11. The velocity field cross section is close to the expected Poiseuille profile, with little variation in profile at the different x locations. The colored contour shading included in Fig. 11 helps us illustrate this similarity.

V. CONCLUSIONS

In this paper the viability of x-ray PIV has been further demonstrated. Furthermore we have highlighted several flaws in the approach of investigators who have previously used x-ray PIV to measure 2D velocity vector fields of flows that vary over z.

We have demonstrated a useful technique for extrapolating correct 2D vector fields and correlation peaks. This allows not only accurate measurement of 2D vector fields but also interrogation of correlation peaks corresponding to velocity probability distribution in the z direction.

Under certain circumstances, this PDF can be used to infer the velocity profile over z. In this case, Poiseuille flow through a pipe has been measured in a 3D sense.

The authors anticipate that in the future similar measurements can be made with fewer or no assumptions about the nature of the flow, by extracting additional information during image acquisition. The most likely method for gaining this information would be through the measurement of the flow volume from multiple perspectives. This technique would combine the advantages of both SPIV and x-ray computed tomography.

ACKNOWLEDGMENTS

The authors gratefully acknowledge the support of the Japan Synchrotron Radiation Research Institute (JASRI) (under Proposal No. 2006A0002) and David Vine for his helpful assistance conducting experiments. Support from an Australian Research Council Discovery Grant (DP0555897) is also gratefully acknowledged.

[1] R. Ross, Nature (London) **362**, 801 (1993).
[2] J. Radermacher *et al.*, N. Engl. J. Med. **344**, 410 (2001).
[3] J. E. Moore, C. Xu, S. Glagov, C. K. Zarins, and D. N. Ku, Atherosclerosis **110**, 225 (1994).
[4] A. S. Anayiotos, S. A. Jones, D. P. Giddens, S. Glagov, and C. K. Zarins, J. Biomech. Eng. **116**, 98 (1994).
[5] X. He and D. N. Ku, J. Biomech. Eng. **118**, 74 (1996).
[6] D. N. Ku and D. P. Giddens, J. Biomech. **20**, 407 (1987).
[7] J. Zhang, B. Tao, and J. Katz, Exp. Fluids **23**, 373 (1997).
[8] Y. Pu and H. Meng, Exp. Fluids **29**, 184 (2000).
[9] C. Brucker, Meas. Sci. Technol. **8**, 1480 (1997).
[10] T. Hori and J. Sakakibara, Meas. Sci. Technol. **15**, 1067 (2004).
[11] A. Seeger, K. Affeld, L. Goubergrits, U. Kertzscher, and E. Wellnhofer, Exp. Fluids **31**, 193 (2001).
[12] S.-J. Lee and G.-B. Kim, J. Appl. Phys. **94**, 3620 (2003).
[13] S.-J. Lee and G.-B. Kim, J. Appl. Phys. **97**, 064701 (2005).
[14] C. D. Meinhart, S. T. Wereley, and M. H. B. Gray, Meas. Sci. Technol. **11**, 809 (2000).
[15] M. G. Olsen and R. J. Adrian, Exp. Fluids **29**, S166 (2000).
[16] R. A. Lewis, Phys. Med. Biol. **49**, 3573 (2004).
[17] R. A. Lewis , N. Yagi, M. J. Kitchen, M. J. Morgan, D. Paganin, K. K. W. Siu, K. Pavlov, I. Williams, K. Uesugi, M. J. Wallace, C. J. Hall, J. Whitley, and S. B.Hooper, Phys. Med. Biol. **50**, 5031 (2005).
[18] R. J. Adrian, Annu. Rev. Fluid Mech. **23**, 261 (1991).
[19] C. Willert and M. Gharib, Exp. Fluids **10**, 183 (1991).
[20] H. Huang, H. E. Fiedler, and J. J. Wang, Exp. Fluids **15**, 263 (1993).